cogent engineering

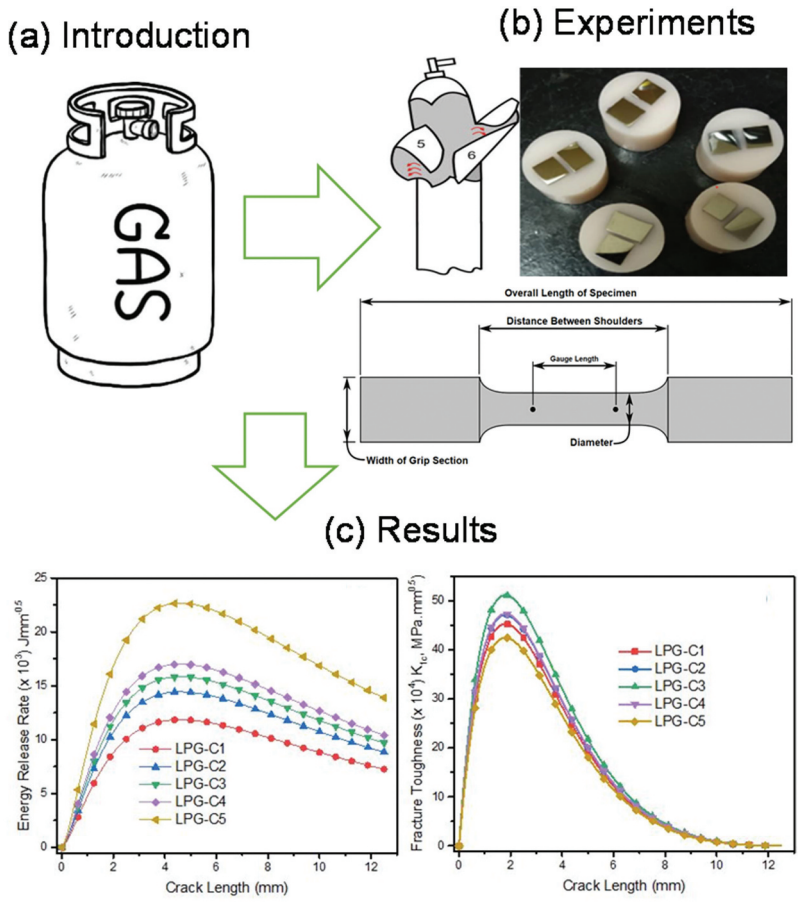

Comparative analyses of the mechanical and microstructural properties of the weld region of LPG cylinder materials

Beatrice Ardayfio, John Ekow Ampah-Essel, William Tetteh, Joshua Asante Tuah, Benjamin Agyei-Tuffour, Kofi Ahomka Annan, Bismark Mensah, Emmanuel Nyankson and David Dodoo-Arhin

Cogent Engineering (2023), 10: 2219096

Ardayfio et al., *Cogent Engineering* (2023), 10: 2219096
https://doi.org/10.1080/23311916.2023.2219096

cogent engineering

MATERIALS ENGINEERING | RESEARCH ARTICLE

Comparative analyses of the mechanical and microstructural properties of the weld region of LPG cylinder materials

Beatrice Ardayfio[1], John Ekow Ampah-Essel[1], William Tetteh[1], Joshua Asante Tuah[1,2], Benjamin Agyei-Tuffour[1]*, Kofi Ahomka Annan[2], Bismark Mensah[1], Emmanuel Nyankson[1] and David Dodoo-Arhin[1]

Received: 04 April 2023
Accepted: 21 May 2023

*Corresponding author: Benjamin Agyei-Tuffour, Department of Materials Science and Engineering, University of Ghana, Off Anne Jiaggi Road, P. O. Box LG 77, Accra, Ghana
E-mail: bagyei-tuffour@ug.edu.gh

Reviewing editor:
Tanveer Saleh, Metallurgy & Materials, The University of Birmingham, Birmingham, UK

Additional information is available at the end of the article

Abstract: This paper presents the numerical and experimental results of the mechanical and microstructural properties of liquefied petroleum gas cylinders from local sources. The tensile strength, burst and fracture toughness of the materials were also investigated. The results show that the carbon content for all samples averaged ~0.22 wt% and manganese ~0.76 wt% and the microstructure was largely pearlitic. The tensile strength showed that LPG-C3 recorded high tensile strength of ~ 611 MPa and hardness of ~ 200 HV while LPG-C5 recorded low tensile strength of ~ 450 MPa. The finite element analysis (FEA) showed fracture toughness of $\sim 5 \times 10^5 MPa.mm^{0.5}$ for LPG-C2 and the energy release rate of $\sim 2 \times 10^6 J/m^2$ for LPG-C5. All samples exhibited high resilience to crack propagation which showed ductile fracture after tensile test. The implications of the results are discussed to elaborate on the influence of carefully controlling the alloying elements of LPG cylinder materials on their mechanical and microstructures during fabrication.

ABOUT THE AUTHORS

Benjamin Agyei-Tuffour, Beatrice Ayeley Ardayfio, John Ekow Ampah-Essel, Bismark Mensah, Emmanuel Nyankson and David Dodoo-Arhin are researchers in the Department of Materials Science and Engineering. The research interests are in manufacturing engineering, mechanical behavior, fracture and crack behavior in materials and organic/perovskite solar cells.
William Tetteh completed MPhil in Materials Science and Engineering, University of Ghana and works with the Ghana Cylinder Manufacturing Company (GCMC) in Ghana as the Technical Engineering Manager
Kofi Ahomka Annan and Joshua Tuah Asante are with the University of Pretoria and research into materials engineering of metals and alloys for structural application.

PUBLIC INTEREST STATEMENT

The use of Liquefied Petroleum Gas (LPG) as fuel source in both domestic and industrial applications has seen considerable increase because governments have made efforts to adopt clean energy policies to mitigate climate change effects. The containers often used to store and/or transport the LPG are manufactured using welded pieces and these weld joints often act as the weak paths during failure and accidents that cause loss of human lives and properties. This study investigates the role that the weld joints, its microstructure and mechanical properties play in improving the fracture toughness of the LPG cylinder and resisting catastrophic failures during accidents. The findings would give the public a comprehensive understanding of the failure mechanisms of LPG cylinders, the choice of LPG cylinder during acquisition and the appropriate ways of handling LPG cylinders in ways to minimize accidents in both domestic and industrial settings.

Subjects: Composites; Materials Processing; Metals & Alloys; Surface Engineering-Materials Science

Keywords: Gas cylinder materials; weld-region; burst test; microstructures; fracture toughness

1. Introduction

Liquefied Petroleum Gas (LPG) is a safe and reliable energy source for domestic and industrial applications (Amorin & Dabo, 2022; Kahangamage et al., 2022). The cylinder materials should possess superior mechanical properties to enable safe storage and use [Susmitha et al., 2022], transport and minimize accidents (Shahrier et al., 2020). Materials that have been used to produce cylinders include steel alloys (Tom et al., 2014), aluminum and glass fiber-reinforced polymer composites . The fabrication techniques include cold flow forming, used for large diameter cylinders, hot deep drawing method, two- and three-piece weld cylinder for small diameter cylinders.

Prior studies have reported steels to be the dominant cylinder material in the manufacturing of LPG cylinders despite its attendant overweight and corrosion susceptibility which results in leakages and explosions. Aluminum and glass fiber epoxy composites have also been used because for example, Aluminum 6061-T6 and 5052-H38 alloys were proposed in 2020 in place of steels due to their light weight and corrosion-resistant properties. Previous investigation reported that glass fiber epoxy composites having showed great promise as alternative to steels with their high specific stiffness/modulus approximately 0.01310 GPa.m^3/kg, specific strength approximately 0.0490 m^3/Kg, and energy absorption capacity approximately 180 kJ/kg (Jacob et al., 2001).

Relatively, the high cost of the alternative materials for cylinder manufacturing keeps steel as the steels more sustainable, reliable and dominant cylinder materials. The parameters adopted for cylinder manufacturing play integral roles in the mechanical and microstructural characteristics of the cylinder. Prior studies have reported on two- and three-piece cylinder techniques in which two and three pieces of the same materials are welded together into the cylinder. During welding, the heat-affected zone (HAZ) often has different microstructure and mechanical properties from the parent material. There exist high internal/residual stresses in the entire cylinder material.

Welding in cylinders includes the Gas Tungsten Arc Welding (GTAW) Kumar and Shahi (2011), Shielded Metal Arc Welding (SMAW) and Submerged Arc Welding (SAW) (Fan et al., 2021; Wang, 2017). Whereas the GTAW technique requires low, mid low and high heat inputs. SMAW and SAW welds are well known for their low heat input as in the case of low temperature high manganese steel (Fan et al., 2021; Singh & Singh, 2019). With these different techniques, the properties of importance include high ultimate tensile strength (UTS) at ~2.56 kJ/mm energy input, high grain coarsening in the HAZ, austenitic microstructure, etc. and upon comparison, welded joints from SMAW exhibit superior tensile strength of ~ 773 MPa and elongation ~ 30%. SAW has recorded UTS of ~ 713 MPa and elongation of 24% at room temperature according to Fan et al. (2021) and Yu et al. (2020)).

Aside the important mechanical properties of the cylinder materials, the microstructural properties of the weld regions after the manufacturing process are also very critical (Xiao et al., 2020). In the manufacturing of LPG cylinders, hot deep drawing or cold flow forming are the commonest methods used. These techniques result in fine surface finish, high tolerance of size and improved fatigue lives (Li et al. (2019). Heat treatment processes such as hardening and tempering after welding stages have an effect on the mechanical properties of cold flow formed AISI 4130 (Far et al., 2019). These microstructural property changes are due to thermal recovery and recrystallization leading to non-distinct orientation of the grains (Li et al., 2019).

Serindag *et al*. (2022) and Gong et al. (2022) reported an U71-Mn rail steel-welded joint and their microstructures showed a fully pearlitic with the HAZ region showing both pearlitic and ferritic

structures. The presence of manganese, molybdenum and chromium caused a significant change in the microstructure, with no dendritic grains in the welded zone. Panigrahi et al. (2009), Celada-Casero et al. (2019), Far et al. (2019) showed that copper, phosphorus and chromium (low concentrations) in low carbon steel form martensitic structures in chloride environments. This is because the M_S temperature for steels with low carbon is higher and the driving force necessary for the transformation to martensite in low carbon steel is smaller.

Prior studies have used the combination of experimental and finite element modeling techniques (FEA) to greatly improve the understanding of the mechanical and microstructure effects of welding on cylinder materials. The FEA provides a visualized stress concentration and distribution in the welded region and their effects on fracture toughness and failure mechanisms (Svitlana Kalmykova (2021)). Compressive and tensile loads are usually applied to the welded joint to investigate the residual stresses and percentage elongation which has been well presented in the past. A study by Subramaniyan et al. (2022) reported similar results in tensile strength and % elongation when a GTAW butt weld of Ti-6Al-4 V sheet (~16 mm) was produced experimentally and compared with numerical results. Similar studies have been reported for thermal distributions; distortion and residual stresses in a GTAW-welded steel plate (Logesh et al., 2022) and tensile strength, elongation and Youngs modulus for a laser-welded piece (Reisgen et al., 2011). The experimental results have often agreed with the numerical results. Therefore, finite element modeling is an important tool used in predicting the mechanical properties of welded LPG joints. These analyses are largely missing in the LPG cylinders locally produced and therefore, the need to correlate the experimental results with the finite element analyses of the mechanical and microstructural properties cannot be overemphasized.

In this paper therefore, samples of LPG cylinders from various local sources which have varying manufacturing parameters and therefore varying resistances to failure during operation have been investigated. In this paper therefore, the chemical composition, microstructural, burst test, tensile, fracture toughness properties, are investigated and compared. Using analytical and numerical model with fracture mechanics concepts, the effects of surface cracks and crack growth on the fracture toughness and energy release rate are also investigated. The authors are not aware of any studies that have compared the mechanical and microstructural properties of the weld region of different of LPG cylinder source materials for a holistic understanding of their responses during accidents. Hence, the findings will greatly enhance the understanding of the material properties and their influence as effective LPG storage and transport materials in homes and industry across Africa and the world.

2. Theory

The LPG cylinder during use experiences cyclic loading from the gas molecules. The loads induced on the surfaces of the cylinder material often results in open cracks which can be detrimental to the life of the cylinder and users. The rate at which cracks propagate through the material is imperative to reduce its failure. As the crack initiates in the steel's surface, the material builds a resilience (fracture toughness (K_{IC})) to reduce the propagation of the crack as in Equations 1–9. In some cases, the energy of resilience is less than that of the energy produced by the tip of the open crack leading to crack propagation usually at a faster rate; this energy produced at the tip of the crack is known as Energy Release Rate (G). To estimate the fracture toughness and the energy release rates, Matlab Simulink and finite element modeling using the ABAQUS CAE were adopted in this study. The low carbon steel that was employed in the simulations is shown to have elastic properties in Table 1.

This energy release rate is derived for a steel material below:

$$K_{IC} = Q = R \tag{1}$$

$$K_{1C} = Y\sigma\sqrt{\pi a} \tag{2}$$

$$R = Y\sigma\sqrt{\pi a} \tag{3}$$

$$\sigma = F_{\max} \tag{4}$$

where $F_{\max}$ is maximum applied load to induce fracture

The energy release rate is calculated as E* which is the plain strain young's modulus

$$G = \frac{1}{E^*}\left(K_I^2\right) \tag{5}$$

where $E^* = \frac{E}{1-\upsilon^2}$G = G_C = R, and G_C = critical energy

$$G = \frac{1}{E^*}\left(Y\sigma\sqrt{\pi a}\right)^2 \tag{6}$$

Prediction of critical energy release rate is as follows:

$$\frac{\Delta G}{G} = \frac{\tan^2\left\{1 - k\left[a_o\left(1+\tan^2\psi\right)\left(\frac{\Delta G}{G}+1\right)\right]\right\}}{1+\tan^2\psi} \tag{7}$$

$K(a) = \frac{1}{\lambda}, a_o$ is materials parameter, H = height of interface step, D = facet length, l = facet center spacing

$$a_o = \frac{\pi E H^2 / l G_o}{32(1-\upsilon^2)\ln(1/\sin(\pi D/2l)} \tag{8}$$

$X = \frac{EH}{G_o}$ where X provides basic information of contact zone dimension where large values of X (~10) associates to maximum contact and small value of X (~0.10) associates to lack of contact. In the case of large X values, our energy release rate equation is as follows:

$$G = G_o\left(1+\tan^2\psi\right) \tag{9}$$

3. Materials and methods

3.1. Cylinder material sources and chemical composition

The LPG cylinder sources were acquired from five cylinder brands in Ghana as presented in Table 1. Chemical analysis test specimens of 10 mm × 10 mm were cut from each cylinder brand using the

Table 1. Chemical composition of cylinder source materials

Steel	C	Si	Mn	S	P	Nb	Ti	V
LPG-C1	0.21	0.05	0.80	0.01	0.02	0.03	0.001	0.004
LPG-C2	0.08	0.26	0.52	0.02	0.04	0.04	0.001	0.000
LPG-C3	0.22	0.27	0.75	0.01	0.06	0.04	0.002	0.006
LPG-C4)	0.20	0.16	0.35	0.01	0.04	0.03	0.002	0.004
LPG-C5	0.15	0.53	0.81	0.02	0.01	0.03	0.002	0.005
ISO 9809–1	0.3–0.37	≤0.4	0.60–0.90	≤0.35	≤0.035	0.9–1.2	<0.15	<0.30

Zip 2 plasma cutter and polished using grinding stone of varying coarse to fine grit sizes. This was done to clean all dirt and make smooth the sample surfaces. The chemical composition of the specimens was measured using the Solarix mass spectrometer (Solarix, Italy) and numerical modelling carried out using Abaqus CAE.

3.2. Tensile and hardness tests

The two mechanical tests done are tensile test and hardness test. Rectangular specimens (20 mm × 120 mm) for the tensile test were cut out of the cylinders in the longitudinal and transverse directions of the weld zone using the Plasma cutting machine (Zip 2.0, Air Liquide, France). The specimens were flattened at room temperature while ensuring negligible work hardening takes place. This was done to avoid impediments posed by the natural curvature of the cylinder to the tensile pull and also the distorted condition of the materials. The tensile tests were done in accordance with EN 10,204 3.1 standard whilst the hardness tests were carried out according to ISO 6506 standard.

3.3. Burst tests

In order to measure the burst resistance of the cylinders, new and unused 6 kg cylinders were subjected to varying pressure to determine the pressure at which the cylinder failure occurs. A single-acting hydraulic pump was used to control the pressure while the cylinder specimen was filled with water. The cylinders were placed vertically during the experiments and air was vented during the filling.

3.4. Microstructural study

Samples for microstructural analyses were prepared weld regions of the cylinders in 10 mm × 10 mm dimensioned pieces using a hack saw and subjected to relevant treatment steps to make surfaces scratch-free. The specimens were cold-mounted overnight using the Leco Acrylic resin and a hardener. The Leco GP − 25 Grinder, polisher and silicon carbide papers were used to rough grind sample surfaces, starting with the silicon carbide paper grit 120, 180, 240, 320, 400 and 600 consecutively. The samples were rotated between 0 and 90° during the grinding and polishing. The coarsely grounded surfaces were polished with diamond paste ranging from 6-micron to 1-micron diamond paste. A polishing cloth which used lapping oil in lieu of water was used to finalize the polishing process. These polished samples were etched in 2% Nital solution following the ASTM E 407–07 standard. The polished samples were observed under the SEM and Olympus B×51 M optical microscope. Image-j ® software was used to calculate the percentage of pearlite in all the samples using the threshold of the 8-bit images.

3.5. Finite Element Modeling (FEM)

To better comprehend the interplay between the loads applied on the steel material when using the cylinder, finite element modeling (FEM) was carried out (Dassualt Systems Simulia Corporation, Providence RI). Meshing was done using a four-node elemental mesh and ensured fine meshes were used in areas of high load interaction was perceived. To ensure a stable simulation, the top and bottom boundaries were fixed and uniform load was applied to the mid-section. The stress distribution of the steel material was estimated using the von Mises stress yielding criterion. For this study, a steel material with low carbon content was used together with the elastic properties as shown in Table 2.

4. Results and discussion

4.1. Chemical composition

The results of the chemical composition tests of the samples are compared to the tolerable maximum for each element according to ISO 22,991 in Table 1. The samples (LPG-C1-LPG-C5) recorded chemical contents within the acceptable standard ranges for steel grades required for LPG cylinder fabrication. Maharjan et al. (2020) have described the prominent influences of steel composition, precisely the effect of carbon (C) on the functioning of the part. Sample LPG-C2

Table 2. Material property used for modeling

Type of steel	E (GPa)	Poisson's ratio
Low Carbon Steel	230	**0.3**

showed a relatively lower carbon content than the other four samples. Consequently, it is expected to show relatively lower strengths, lower amount of cementite phases in the pearlite structure and higher ductility. Increased carbon content is as such required to guarantee the appropriate mix of strength and ductility. Silicon (Si), known as one of the principal deoxidizers in steel increase the soundness by making it free from defects, decays or damages. Da Silva et al., (2016) have reported the increase in strength of double-phase steels after annealing and upon addition of silicon. High volumes of very hardenable homogeneous austenite are shown to be formed with slow cooling, which further increases the volume of martensite in the final structure. This further increases the strength and hardness but to a lesser extent than manganese. Although to a lower amount than carbon, manganese increases the tensile strength and hardenability of steel. However, very high carbon with very high manganese enables embrittlement. It is therefore optimum to keep manganese content between ~ 0.30% and ~ 0.76%. Samples LPG-C2 and LPG-C4, from Table 4.1, have manganese content of ~ 0.408% and ~ 0.282%, respectively, which implies a high possibility of containing internal porosity and crack during welding. Additionally, the appropriate micro-alloying with elements such as niobium, titanium, vanadium and boron in high strength LPG grade steels coupled with thermos-mechanical processing can provide excellent combination of high strength and ductility. The chemical compositions therefore have an effect on the microstructure of the various steels as well as the tensile, hardness and burst results as shown in the sections following.

4.2. Microstructures

Figure 1 presents the optical micrographs of all samples LPG-C1–LPG-C5 (Figure 1(a-e)). The microstructure is mostly made up of ferrite grains and regions of pearlite structures at grain boundaries, grain corners and few grains. The ferrite phases are the light patches, whereas the pearlite phases are the grey patches comprising of alternating layers of ferrites and cementite. From the results, it is shown that the percentages of pearlite structure in the various samples are ~ 30.6, ~ 8.9, ~ 47.9, ~ 6.2 and ~ 9.9% for LPG-C1, LPG-C2, LPG-C3, LPG-C4 and LPG-C5 samples, respectively. The amount of pearlite is affected by the carbon content of the material used (Mates et al. (2016)). This is because carbon diffuses more into the steel during slow cooling and hence the ferrite transforms to cementite which is a component of the pearlite structure. Similarly, upon tempering of a martensite structure, carbon diffuses into the steel and hence transforms to cementite, S. Li et al. (2022). From the chemical analysis, it is seen that the results correspond to that shown for pearlite percentages with sample LPG-C3 showing the highest carbon content of ~0.22 wt% and highest pearlite percentage of ~ 47.9%. This amount of pearlite in the structure affects the mechanical properties such as hardness and tensile properties. The micrographs show that the samples from sample LPG-C4 are made of very fine pearlite structures whereas that of sample LPG-C3 is made of very coarse pearlite structures. There is a relation between the inter-lamellar spacing of pearlite (that is how fine or coarse the pearlite structure is) and the mechanical properties. Interlamellar spacing is a very important parameter in steels composed of the pearlitic structure. As the interlamellar spacing becomes finer, the pearlite structure is seen to be finer and the strength, toughness and ductility all increase (Vander Voort et al, 2015).

Globular structures instead of lamellar structures are observed due to the inadequate cooling time to allow segregation (Pandey et al., 2019). The presence of micro-alloying elements in the steel is attributed to the limited recrystallization and grain growth during hot rolling process. This process refines the final austenite grain structures and creates prolific nucleation of ferrite during cooling which results in extra refinement of the final grain structure. The precipitation of micro-

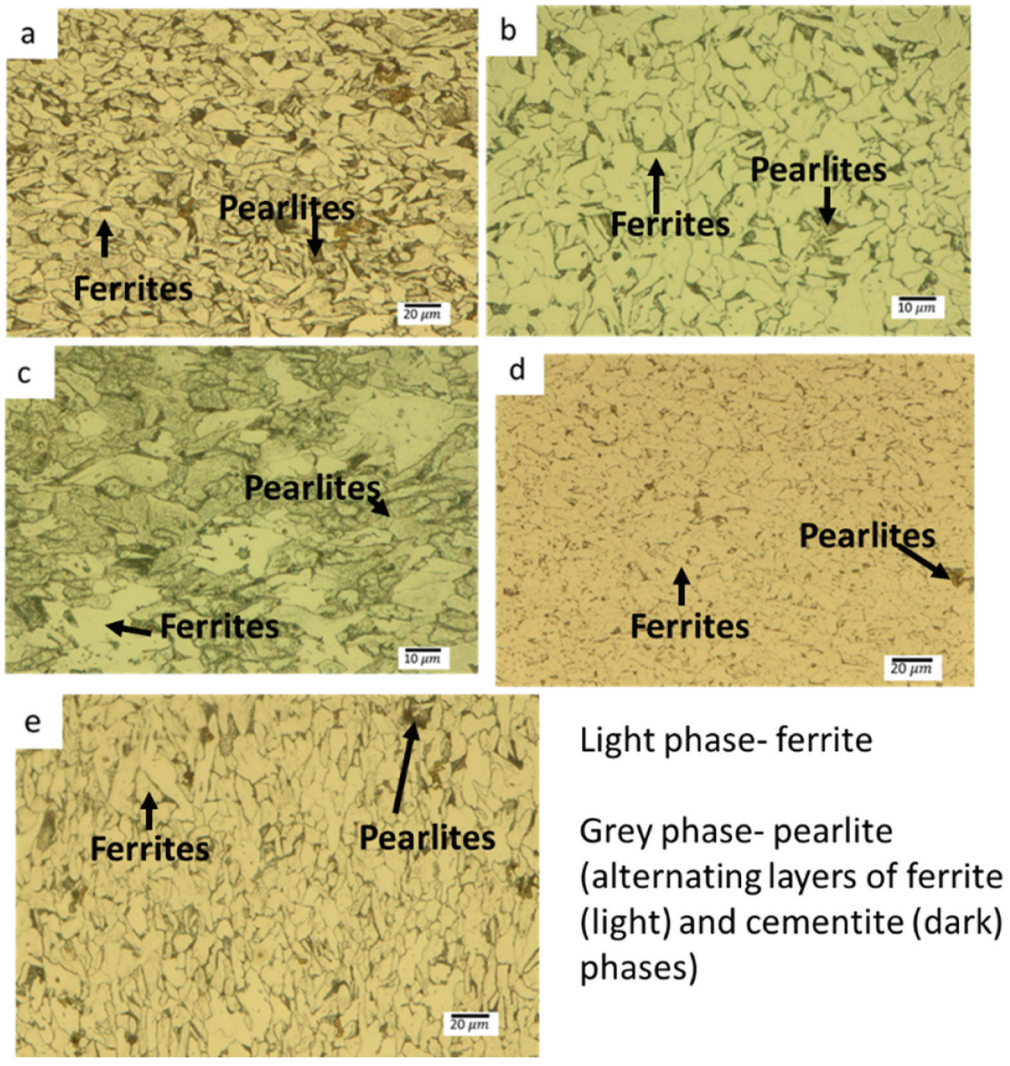

Figure 1. Optical micrographs of the samples (a) LPG-C1, (b) LPG-C2, (c), LPG-C3, (d) LPG-C4 and (e) LPG-C5.

alloy carbides and nitrides also takes place since these phases are much less soluble in ferrite than in austenite. This provides further strengthening by formation of finely dispersed particles.

The fractured surface of the samples was examined in a JEOL SEM. Figure 2 shows the morphology of the fractured surface of the samples after the tensile tests. All the samples failed in a ductile manner as shown by the micrographs.

4.3. Mechanical properties

4.3.1. Hardness and tensile properties

Table 3 reports on the mechanical properties of the various cylinder material sources. From the results, it is seen that all cylinder material sources recorded values in between the recommended standard for the test according to ISO 22,991. Table 3 shows that samples LPG-C3 recorded the highest hardness, tensile and yield strength while sample LPG-C5 recorded the least hardness, tensile and yield strength. This corresponds to the chemical composition and microstructural analysis. Sample LPG-C3 contains the highest carbon content amongst all the other materials, therefore the higher ability for formation of pearlites. Also, the interlamellar spacing in sample LPG-C3 is seen to be finer from the microstructures than for the other samples. Figure 3 illustrates

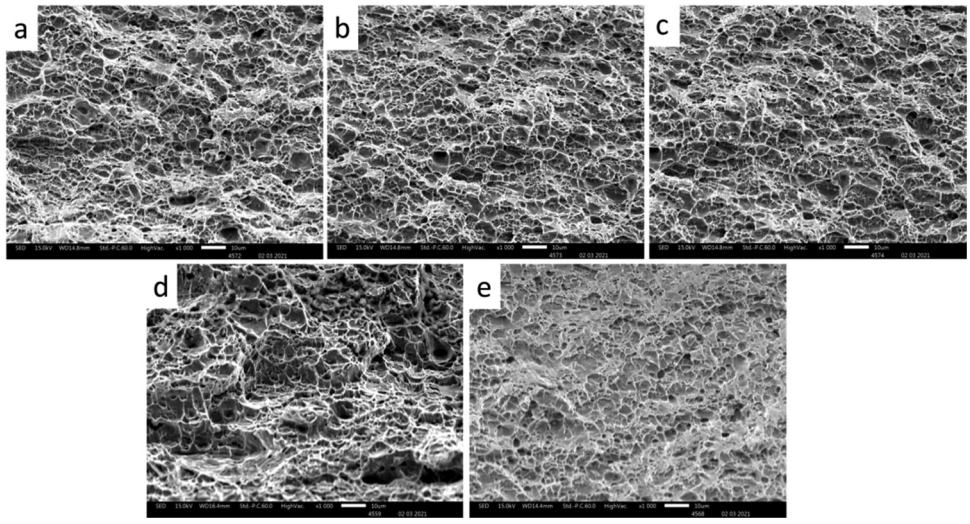

Figure 2. SEM micrographs of the fractured surface showing the ductile behavior of all the samples (a) LPG-C1 (b) LPG-C2, (c) LPG-C3, (d) LPG-C4 and (e) LPG-C5.

stress-strain curves from the different LPG cylinder samples of manufacturers. After testing, LPG-C3 recorded ~ 600 MPa, LPG-C5 of ~ 450 MPa being the highest and the least tensile strengths, respectively. Changes in curves are attributed to the presence of the alloying elements, mainly carbon. An increase in carbon content results in dislocation motion hindrance in steels. These results agree with prior work by Odiaka et al. (2020).

The hardness results show that LPG-C3 recorded ~ 200 HV as the highest and LPG-C5 with 165 HV as the least. The hardness and tensile strength value differences are due to the presence of manganese and carbon in the different source materials. The alloying and compositional elements also have an effect on the hardness and tensile properties of the manufacturing material used according to Chang et al. (2020). The cumulative results of the mechanical tests performed are shown in Table 3.

4.4. Burst test analysis

The burst test response of the cylinder samples is shown in Table 4. The burst pressure for all the samples was higher than the ISO 22,991 minimum ~ 5.0 MPa. Sample LPG-C1 recorded the highest pressure of ~ 12.4 MPa with the least ~ 11.5 MPa for Sample LPG-C4. The average burst pressure across the samples was ~ 12.0 MPa at an average ~ 11.5% volumetric expansion. Sample LPG-C2, however, recorded a very low (~6.3%) volumetric expansion and sample LPG-C5, with ~ 19.5% as the highest. The differences observed in the volumetric expansion of the finished cylinders are function of the source materials used as well as the adequacy of the heat treatment parameters such as furnace soaking time and cooling time during their manufacturing processes according to Ramakrishna *et al*., (2013). Figure 4 shows the image and position of the crack after the burst test. They confirm that the crack did not initiate from the weld region as represented in Table 4.

Table 3. Mechanical test results for cylinder sources

Sample	Tensile strength/MPa	Yield strength/MPa	Modulus/GPa	Elongation/%	Hardness/HV
LPG-C1	583.8 ± 65	376 ± 42	311.5 ± 23	17 ± 4	189.9 ± 8.7
LPG-C2	578.3 ± 58	389 ± 46	253.6 ± 21	14 ± 3	200.1 ± 10.5
LPG-C3	611.3 ± 66	418 ± 54	232.4 ± 18	9 ± 2	201.7 ± 13.5
LPG-C4	558.6 ± 45	392 ± 45	217.1 ± 16	15 ± 3	181.4 ± 10.6
LPG-C5	525.6 ± 60	352 ± 40	162.9 ± 12	23 ± 6	165.9 ± 7
ISO 22,991	241–2450	140–2400	183–213	3.00–48.0	22.0–661

Figure 3. Stress-strain curves for various cylinder material sources.

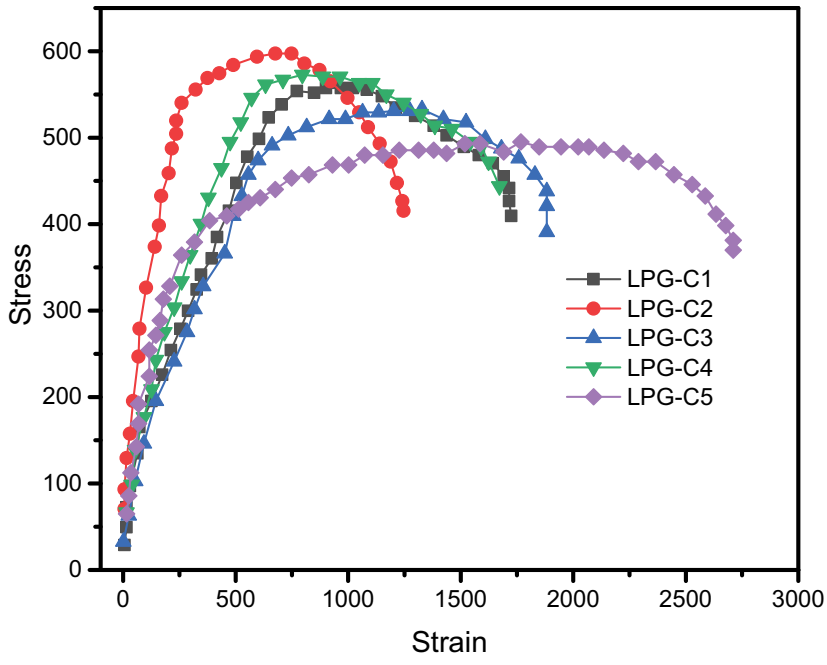

4.5. Finite element analysis

4.5.1. Tensile stress analysis

Figure 5 shows the von Mises stress distributions with color representations and failure modes of the different steel LPG source materials under tensile stress. It is noticed that the stress effect was mostly intense at the middle section as load is applied to the steel sample. The red coloration shows necking at the region where failure subsequently occurs, which is very characteristic of steel samples with significantly high carbon percentage. From Table 1, it can be observed that LPG-C3 (0.22 wt%) had the highest carbon present with LPG-C2 (0.08 wt%) recording the least.

4.5.2. Burst test analysis

Figure 6 presents the von Mises stress distributions under increasing subjected load. The cylinder is noticed to record higher stress at the top part upon application of internal pressure as the color contours present. Finite element analysis (FEA) was used to evaluate the burst pressure of mild steel pressure vessel using Ramberg-Osgood model. This proceeded to necking and eventually failure. This phenomenon was also evident in experimental burst tests conducted. The burst pressure in this sense is observed to the minimum pressure that caused irreversible damages in the cylinder body (see Figure 6b). It was calculated considering zero external pressure with no axial loading; therefore, the force required to burst the cylinder from the inside is counteracted only by the strength of its steel walls.

4.5.3. Fracture toughness, energy release rate and crack length

A material under constant load undergoes mechanical deformation and this deformation may be elastic or plastic but as it undergoes the changes existing voids/notches tend to propagate, leading to rapture and fracture in most cases. But all materials have in built toughness which helps them to some extent resist these deformations. The toughness to fracture is represented mathematically as $K=Y\delta\sqrt{\pi a}$ which is dependent on the stress applied and the length of crack present in the material. During the toughening of the material to resist failure, it releases energy which is also represented mathematically as $G=\frac{k_1^2}{E^1}$, where k is the stress intensity factor and E is the stress applied in the direction of the force.

Table 4. Burst test results

Sample	Burst Pressure (MPa)	Volumetric Expansion (%)	Crack Initiation
LPG-C1	12.4	11.3	Fracture did not initiate in the weld
LPG-C2	12.2	6.3	Fracture did not initiate in the weld
LPG-C3	11.8	13.8	Fracture did not initiate in the weld
LPG-C4	11.5	6.5	Fracture did not initiate in the weld
LPG-C5	12.2	19.48	Fracture did not initiate in the weld

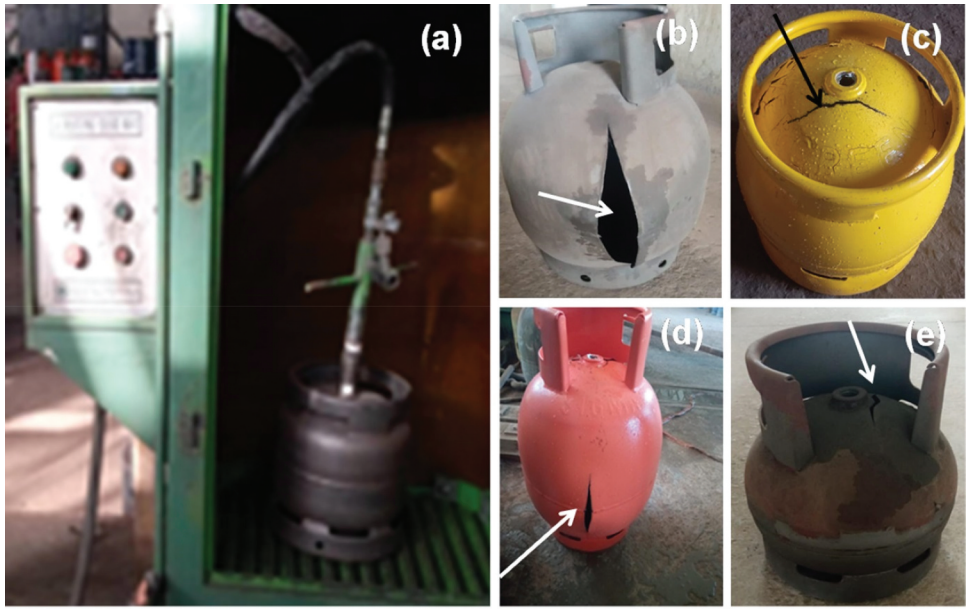

Figure 4. Shows the burst testing technique (a) and position of crack relative to welded region in the LPG-C1-LPG-C5 ((b)-(e)).

Figure 7(a) represents the relationship between crack length and the energy released. Energy released by the materials obtained from the different manufacturers showed $2\times10^6 J/m^2$, $15\times10^5 J/m^2$, $14\times10^5 J/m^2$, $13\times10^5 J/m^2$, $8\times10^5 J/m^2$ for (a) LPG-C1, (b) LPG-C2 (c) LPG-C3, (d) LPG-C4 and (e) LPG-C5, respectively. It can be seen that LPG-C1 recorded the highest energy release rate and LPG-C5 recorded the least. The tip of the crack releases energy which causes an increase in energy release rate as shown in the graph; this happens as the length of the crack is also increasing simultaneously. This phenomenon corresponds with Alberto Sapora and A. Doitrands work of which they utilized finite fracture mechanics on notched Brazilian disk samples (Doitrand and Sapora, 2019). It is from the graph that they all thread on the same path at different rates of which energy is released by these cylinders. They are as a result of the conformation to standards, specifically ISO22991.

Figure 7(b) shows the fracture toughness behavior that of (a) LPG-C1, (b) LPG-C2, (c) LPG-C3, (d) LPG-C4 and (e) LPG-C5. By the color representation it is observed that LPG-C2 recorded the highest fracture toughness of $\sim5\times10^5$ MPa.$mm^{0.5}$ with LPG-C5 recording the least with ~42 *MPa*.$mm^{0.5}$. These variations in fracture toughness are as a result of the presence of alloying and compositional elements in the materials used by the different manufacturers. From the mass spectroscopy conducted for compositional analysis, it proved a similarity to the reference standard used

cogent engineering

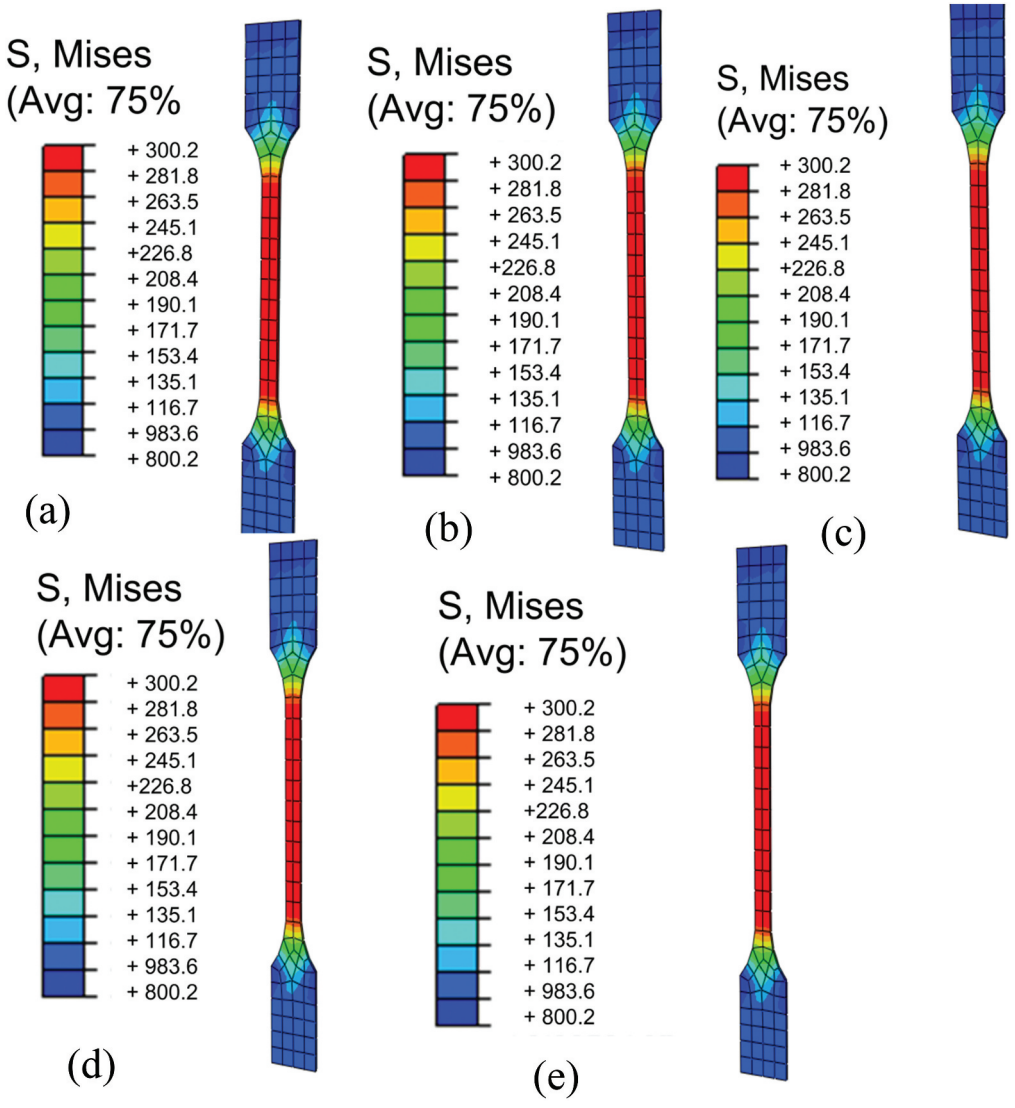

Figure 5. Tensile test models for various cylinder materials (a) LPG-C1 (b) LPG-C2 (c) LPG-C3 (d) LPG-C4 and (e) LPG-C5.

ISO22991 which confirms the variation in fracture toughness. Under similar conditions, Y. Chen et al.'s work demonstrated a slightly different curve which was as a result of the treatment process performed on the material rendering is more brittle than usual. Also Sabah M. Beden et al.'s work under similar conditions arrived at a different curves compared to Y. Chen et al. due to both constant and varying loading to different chemically compositional metallic components under load (Chen 2013; Beden et al., 2009).

Figure 8 shows a progressive propagation of a mode 1 crack type during the tensile loading. In Figure 8a, the crack has been initiated and the tip of the crack is mounting energy to propagate with the help of an external force (tension), in 8(b) a red color contour can be seen at the tip of the crack which indicates high stress levels mounted at that point which is aiding the propagation if the crack moving from a stable region to an unstable region. Beyond this, the catastrophic failure begins where the strength of the material begins to diminish rapidly leading to a distortion in shape as seen in Figures 8(c-d). The blue color contour represents a minimal stress concentration at those regions.

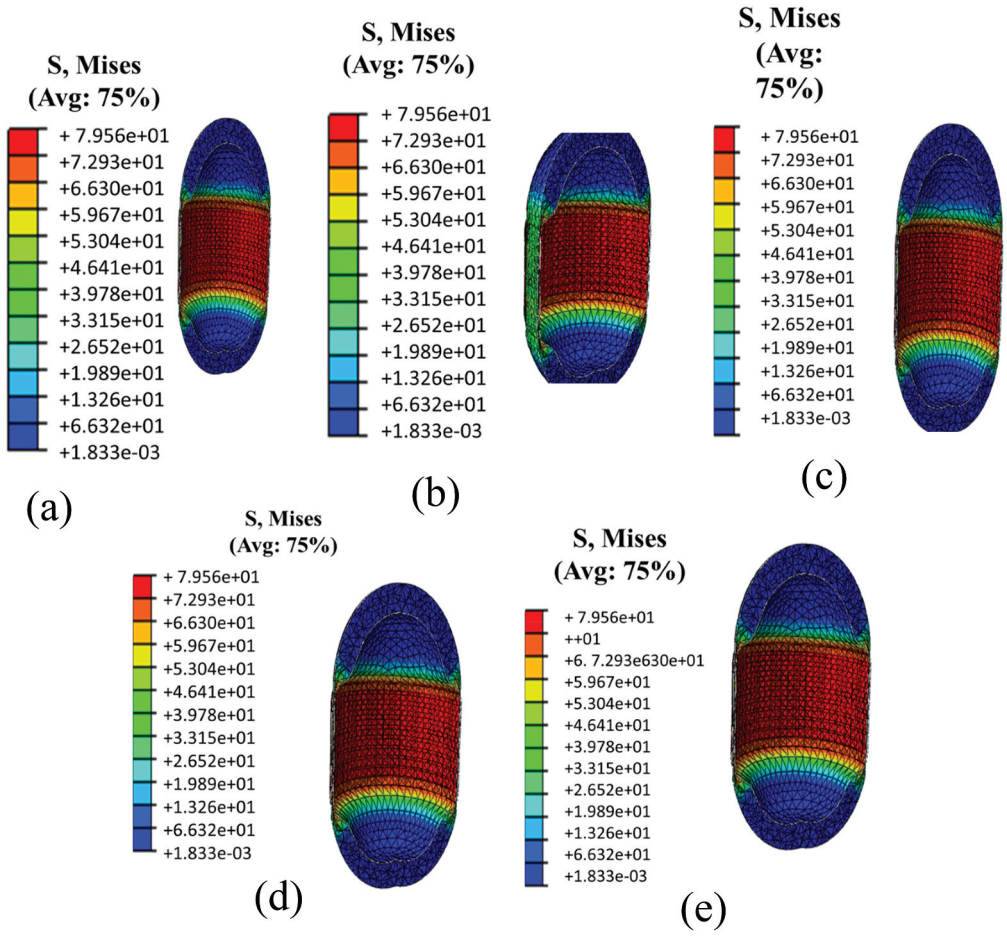

Figure 6. Burst test results for various cylinder material sources (a) LPG-C1, (b) LPG-C2 (c) LPG-C3, (d) LPG-C4 and (e) LPG-C5.

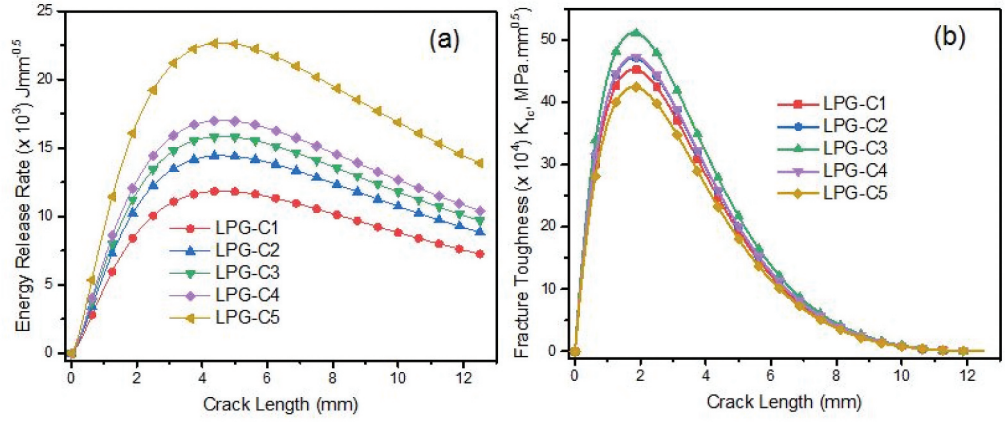

Figure 7. Shows the mechanical properties of samples; (a) fracture toughness and (b) Energy release rate curves.

5. Implications of the results

The above results have significant implications on the manufacturing of LPG cylinders for domestic and industrial uses. First, they suggest that the chemical analysis of the LPG cylinder materials includes acceptable ranges of carbon and manganese, which induces enhanced strength and durability in the cylinders. The microstructures of weld zones recorded similar microstructural images of ferrite and pearlite phases with lamellar structures, but phases present are non-uniform which is explained by inadequate cooling time. Inadequate cooling time leads to

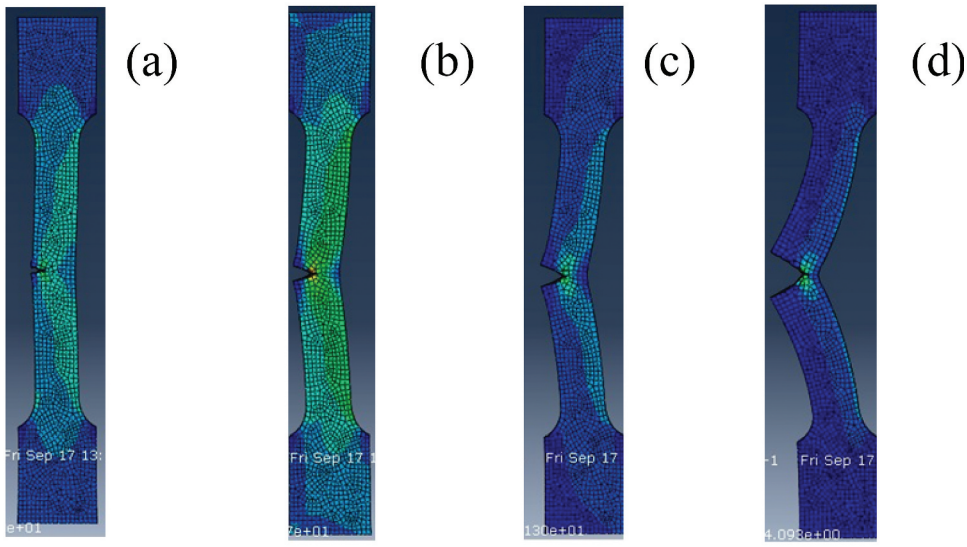

Figure 8. Progression of crack during tensile test of cracked specimen (Models).

incomplete segregation of grain structures. Study recommends micro-alloying elements such as carbides and nitrides be introduced to undergo precipitation of less soluble ferrite to cause extra-refinement of final grain structure. The implication of higher carbon content is seen in the microstructures. Steels with higher carbon content are seen to exhibit higher pearlite phases. In some steels, the interlamellar spaces of the pearlite structure are coarse whiles in other instances, they are small. The smaller the interlamellar spacing of the pearlite structure, the higher the strength, the toughness and ductile properties. The converse is also true and this is confirmed in the mechanical properties as well as models done by FEA. However, the presence of high manganese and carbon could lead to possible embrittlement in the cylinder material. The embrittlement is usually as a result of possible internal porosity and cracks during welding and therefore keeping the manganese content between ~ 0.3% and ~ 0.76% can minimize the embrittlement. Also, increased carbon content can lead to cementite phase formation and subsequently, higher pearlite formation which can impact adversely on the microstructure and mechanical properties. Further work is clearly required to optimize the concentrations of the alloying elements to ensure that robust LPG cylinders that can withstand high stresses and minimize failures are produced.

6. Conclusion and summary remarks

LPG cylinder materials from the local sources were analyzed for their chemistry, microstructures and mechanical properties. High strength and fracture toughened LPG cylinder materials from the local sources are be produced by carefully controlling the alloying elements and microstructures during fabrication. The results from the current experimental and finite element modeling of the LPG cylinder sources suggest that an optimum carbon content of ~0.22 wt% will yield cylinders with enhanced mechanical properties. The tensile strengths showed that LPG-C3 recorded the optimum tensile strength of ~ 600 MPa while LPG-C5 recorded low tensile strength of ~ 450 MPa due to its alloying element, carbon. The fracture toughness of all the samples was very high and above the reported maximum required for fracture toughness of cylinder materials, hence exhibited high resilience to crack propagation. This was evident in the fracture study observed in the SEM micrographs which showed ductile fracture surface after the tensile tests. It is therefore worthy to note that, carefully controlling the alloying elements in the steel affects the microstructures as well as the mechanical properties during fabrication

Acknowledgement
The authors acknowledge the support from the African Research Universities Alliance Early Career Fellowship (ARUA-ECRF), the University of Ghana BANGA-Africa Program, and the TWAS-DFG Fellowship.

Author details
Beatrice Ardayfio[1]
John Ekow Ampah-Essel[1]
William Tetteh[1]
Joshua Asante Tuah[1,2]

Benjamin Agyei-Tuffour[1]
E-mail: bagyei-tuffour@ug.edu.gh
ORCID ID: http://orcid.org/0000-0001-9629-8240
Kofi Ahomka Annan[2]
Bismark Mensah[1]
Emmanuel Nyankson[1]
David Dodoo-Arhin[1]
[1] Department of Materials Science and Engineering, University of Ghana, Accra, Ghana.
[2] Department of Materials and Metallurgical Engineering, University of Pretoria, Pretoria, South Africa.

Disclosure statement
No potential conflict of interest was reported by the authors.

Citation information
Cite this article as: Comparative analyses of the mechanical and microstructural properties of the weld region of LPG cylinder materials, Beatrice Ardayfio, John Ekow Ampah-Essel, William Tetteh, Joshua Asante Tuah, Benjamin Agyei-Tuffour, Kofi Ahomka Annan, Bismark Mensah, Emmanuel Nyankson & David Dodoo-Arhin, *Cogent Engineering* (2023), 10: 2219096.

References

Amorin, R., & Dabo, K. (2022). Assessment of the Safety Handling of Domestic Liquified Petroleum Gas (LPG) cylinders using a suburb of afienya township as a case study. *European Journal of Technology*, *6*(2), 16–31. https://doi.org/10.47672/ejt.1033

Beden, S. M., Abdullah, S., & Ariffin, A. K. (2009). Review of fatigue crack propagation models for metallic components. *28*(3).

Celada-Casero, C., Siestsma, J., & Santofimia, J. (2019). The role of size in the martensitic transformation in low carbon steels. *Materials & Design*, *167*. https://doi.org/10.1016/j.matdes.2019.107625

Chang, G., Zhou, T., Zhou, H., Zhang, P., Ma, S., Zhi, B., & Wang, S. (2020). Effect of composition on the mechanical properties and wear resistance of low and medium carbon steels with a biomimetic non-smooth surface processed by laser remelting. *Metals (Basel)*, *10*(1), 37. https://doi.org/10.3390/met10010037

Chen, Y. (2013). Irradiation effects of HT-9 martensitic steel. *Nuclear Engineering & Technology*, *45*(3), 311–322. https://doi.org/10.5516/NET.07.2013.706

Da Silva Filho, J. F., Oliveira, C. A. S. D., Fonstein, N., Girina, O., Miranda, F. J. F., Drumond, J., Serafim, E. A., & Afonso, C. R. M. (2016). Effect of Cr additions on ferrite recrystallization and austenite formation in dual-phase steels heat treated in the intercritical temperature range. *Materials Research*, *19*(1), 258–266. https://doi.org/10.1590/1980-5373-MR-2015-0641

Doitrand, A., & Sapora, A. Nonlinear implementation of finite fracture mechanics: A case study on notched Brazilian disk samples. (2019). *International Journal of Non-Linear Mechanics*, *119*(May), 103245. 2020. https://doi.org/10.1016/j.ijnonlinmec.2019.103245

Fan, X. L., Y Cai, Y., Qi, X., Wang, Z. and Ma, C., Ma, C. (2021). Mechanical properties of cryogenic high manganese steel joints filled with nickel-based materials by SMAW and SAW. *Materials Letters*, *304*(July), 130596. https://doi.org/10.1016/j.matlet.2021.130596

Far, A. R. H., Anijdan, S. H. M., & Abbasi, S. M. (2019). the effects of increasing Cu and Ni on a significant enhancement of mechnaical properties of high-strength low alloy, low carbon steels of HSLA-100 type. Materials Science and Engineering A, *746*, 384–393. https://doi.org/10.1016/j.msea.2019.01.025

Gong, L., Liu, H., Lv, C., Zhao, L., & Riveiro, A. (2022). Effect of alloying composition on microstructure and mechanical properties of ultranarrow gap welded joints of U71Mn rail steel. *Rivista Italiana della Saldatura*, *74*(1), 1–11. https://doi.org/10.1155/2021/9282463

Jacob, G. C., Fellers, J. F., Simunovic, J. M., & Starbuck, J. M. (2001). Energy Absorption in Polymer Composite Materials for Automotive Crashworthiness. *composite materials*, *36*(7), 813–850. [Online]. Available http://thyme.ornl.gov/composites/reports/jocm01.pdf

Kahangamage, U., Chen, Y., Leung, C. W., & Ngai, T. Y. (2022). Experimental study of lean-burning limits of hydrogen-enriched LPG intended for domestic use. *Journal of Energy and Power Technology*, *4*(2), 1–1. https://doi.org/10.21926/jept.2202016

Kalmykova, S. (2021). "Simulation of T-joints between RHS steel members with offset in Abaqus CAE. *Acta Polytechnica CTU Proceedings*, *30*, 36–40. https://doi.org/10.14311/APP.2021.30.0036

Kumar, S., & Shahi, A. S. (2011). Effect of heat input on the microstructure and mechanical properties of gas tungsten arc welded AISI 304 stainless steel joints. *Materials & Design*, *32*(6), 3617–3623. https://doi.org/10.1016/j.matdes.2011.02.017

Li, Y., Fan, W., Lu, C., Gao, Z., Ma, X., Jin, W., Ye, Y., & Wang, F. (2019). Microstructure and mechanical properties of 34CrMo4 Steel for Gas Cylinders formed by hot drawing and flow forming. *Materials*, *12*(8), 1351. https://doi.org/10.3390/ma12081351

Li, S., He, M., Hu, G., Tian, Y., Wang, C., Jing, B., & Ping, D. (2022). Pearlite formation via martensite, composites part B. *Engineering*, *238*, 109859. ISSN 1359-8368. https://doi.org/10.1016/j.compositesb.2022.109859

Logesh, M., Kumar, M., Shankaranarayana, D. V., Sathyamurthy, R., & Dhanapal, B. (2022). A numerical analysis of friction stir welded joint using FEA. *Materials Today: Proceedings*, *62*, 2362–2369. https://doi.org/10.1016/j.matpr.2022.04.850

Maharjan, N., Zhou, W., & Wu, N. (2020). Direct laser hardening of AISI 1020 steel under controlled gas atmosphere. *Surface & Coatings Technology*, *385* (December 2019), 125399. https://doi.org/10.1016/j.surfcoat.2020.125399

Mates, S., Stoudt, M., & Gangireddy, S. (2016). Measuring the Influence of Pearlite Dissolution on the Transient Dynamic Strength of Rapidly Heated Plain Carbon Steels. *journal Materials Science*, *68*(7), 1832–1838. https://doi.org/10.1007/s11837-016-1951-9

Odiaka, T., Akinlabi, S. A., Madushele, N., Fatoba, O. S., Hassan, S., & Akinlabi, E. T. Statistical analysis of the effect of welding parameters on the tensile strength of titanium reinforced mild steel joints using taguchi's DoE. (2020). *Materials Today: Proceedings*, *44* (December), 1202–1206. 2021. https://doi.org/10.1016/j.matpr.2020.11.240

Pandey, C., Mahapatra, M. M., Kumar, P., Kumar, S., & Sirohi, S. (2019). Effect of post weld heat treatments on microstructure evolution and type IV cracking behavior of the P91 steel welds joint. *Journal of Materials Processing Technology*, *266*, 140–154. https://doi.org/10.1016/j.jmatprotec.2018.10.024

Panigrahi, B. K., Srikanth, S., & Sahoo, G. (2009). Effect of alloying elements on tensile properties, microstructure, and corrosion resistance of reinforcing bar steel. *Journal of Materials Engineering and Performance*, *18*(8), 1102–1108. https://doi.org/10.1007/s11665-008-9336-z

Reisgen, U., Schleser, M., Mokrov, O., & Ahmed, E. (2011). Numerical and experimental investigation of tensile behavior of laser beam welded TRIP700 steel. *Isij*

International, *51*(3), 429–434. https://doi.org/10.2355/isijinternational.51.429

Shahrier, F., Eva, I. J., Afrin, M., Alam, C. S., & Rashid, A. R. M. H. (2020). Literature Review on LCA of LPG as a Transportation and Cooking Fuel. *Proc. Int. Conf. Ind. Mech. Eng. Oper. Manag*, Dhaka, Bangladesh (pp. 1–7). IOEM Society.

Singh, A., & Singh, R. P. (2019). A review of effect of welding parameters on the mechanical properties of weld in submerged Arc welding process, Mater. *Materials Today: Proceedings*, *26*, 1714–1717. https://doi.org/10.1016/j.matpr.2020.02.361

Subramaniyan, M. K., Veeman, D., Nallathambhi, S. S., & Thanigainathan, S. (2022). Gas Tungsten arc welding of Ti-6Al-4V sheet for pressure vessels used in aerospace application: A detailed characterization of weldment. *International Journal of Pressure Vessels and Piping*, *200*(August), 104787. https://doi.org/10.1016/j.ijpvp.2022.104787

Susmitha, P., Arun, P. A., & Sharma, M. (2022). A Study on Safety and Operational Procedures for Filling of Cylinders in an LPG Bottling Plant as per OISD-144. *Advances in Sustainable Development: Proceedings of HSFEA 2020* (pp. 29–39). Springer Singapore.

Tom, A., Pius, G. M., Joseph, G., Jose, J., & Joseph, M. J. (2014). Design and analysis of lpg cylinder. *International Journal of Engineering & Applied Sciences*, *6*(2), 17–17. https://doi.org/10.24107/ijeas.251225

Vander Voort, G. F. (2015). Interlamellar spacingof pearlite. *Practical Metallographie*, *52*(8), 419–436. https://doi.org/10.3139/147.110357

Wang, Z. Q. (2017). Effect of Ni content on the microstructure and mechanical properties of weld metal with both-side submerged arc welding technique, "Mater. *Materials Characterization*, *138*, 67–77. https://doi.org/10.1016/j.matchar.2018.01.039

Xiao, J. K., Tan, H., Chen, J., Martini, A., & Zang, C. (2020). Effect of carbon content on microstructure, hardness and wear resistance of CoCrFeMnNiCx high entropy alloys. *Journal of Alloys and Compounds*, *847*, 156533. https://doi.org/10.1016/j.jallcom.2020.156533

Yu, W. X., Liu, B. X., Chen, C. X., Liu, M. Y., Zhang, X., Fang, W., Ji, P. G., He, J. N., & Yin, F. X. (2020). Microstructure and mechanical properties of stainless steel clad plate welding joints by different welding processes. *Science and Technology of Welding and Joining*, *25*(7), 571–580. https://doi.org/10.1080/13621718.2020.1774995